Pergamon

Adv. Space Res. Vol. 15, No. 8/9, pp. (8/9)137–(8/9)140, 1995

0273-1177(94)00095-6
0273-1177/95 $9.50 + 0.00

A STUDY OF THE SOLAR WIND DECELERATION IN THE EARTH'S FORESHOCK REGION

T.-L. Zhang,* K. Schwingenschuh* and C. T. Russell**

* *Space Research Institute, Graz, Austria*
** *IGPP/UCLA, Los Angeles, CA, U.S.A.*

ABSTRACT

Previous observations have shown that the solar wind is decelerated and deflected in the earth's upstream region populated by long-period waves /1-3/. This deceleration is correlated with the 'diffuse' but not with the 'reflected' ion population. The speed of the solar wind may decrease tens of km/s in the foreshock region. The solar wind dynamic pressure exerted on the magnetopause may vary due to the fluctuation of the solar wind speed and density in the foreshock region. In this study, we examine this solar wind deceleration and determine how the solar wind deceleration varies in the foreshock region.

INTRODUCTION

The deceleration of the solar wind in the foreshock region has been observed by several authors /1-4/. Formisano and Amata /4/ first found a decrease in the solar wind speed in the foreshock region by comparing the observations performed by Explorer 33 and Heos 1. Solar data from ISEE spacecraft have confirmed this perturbation of solar wind properties /1-3/. Bame et al. /1/ have reported that this deceleration is of an average of 7-10 km and it is correlated with the 'diffuse' but not with the 'reflected' ion population. They have suggested that the solar wind deceleration is a result of momentum transfer between the backstreaming ions and the solar wind ions through wave-particle interaction. Furthermore, Bonifazi et al. /2,3/ have noted that the magnitude of the deceleration of the solar wind depends on its bulk speed. Associated with this deceleration of speed, the direction of the solar wind is deflected slightly by around 1°.

Upstream solar wind velocity deceleration and associated density changes may result in pressure perturbations which could create significant effects on the magnetopause /5/. Since the IMF is highly variable in direction, the configuration of the foreshock is subject to change. When IMF changes direction, the foreshock moves and the pressure distribution on the magnetopause moves. Thus even when the upstream solar wind momentum flux is steady, the pressure exerted on the magnetopause may vary due to the variable IMF orientation.

While the foreshock covers a large space in front of the bow shock, the solar wind deceleration may occur in certain parts of the foreshock only. It is our intent to examine the deceleration of the solar wind and determine how this deceleration varies in the foreshock region. This study finds that the solar wind speed decreases most in front of the quasi-parallel bow shock. Along the IMF direction, this deceleration is seen to be a maximum near the bow shock and stops when the distance from bow shock reaches 5 R_E.

OBSERVATIONS

The data used for this study are the ISEE 1 magnetometer measurements and the solar wind data measured by the LASL/MPI crossed-fan solar wind ion experiment in November and December 1977. Both magnetic field and solar wind data were block averaged into 1-min resolution data. In this study, we use the bow shock model of Fairfield /6/ with eccentricity of 1.02, subsolar distance of 14.4 R_E, and focus at X=+3.5 R_E. While the bow shock shape is defined by the Fairfield model, the shock size is extrapolated from the measured solar wind dynamic pressure. Since the bow shock is a 3-D curved surface and the spacecraft position in respect to the foreshock boundary varies with the direction of IMF, we use the "solar foreshock coordinates" /7/ to simplify the geometry to 2-D by assuming rotational symmetry of the shock surface around the X-axis in the aberrated GSE coordinates (with an aberration angle of 4°). In this coordinate system, the x-axis is toward the Sun, the x-y plane is the V-B plane which passes through the location of the spacecraft at a particular time and the bow shock is the cross section of the x-y plane and the 3-D bow shock.
Le and Russell /8/ found that the ULF foreshock starts at where the IMF connected to the shock with a θ_{BN} less than 50°. They showed that the foreshock boundary is well defined in the V-B plane only when the IMF cone angle is greater than 45°. We adopted this definition for ion foreshock with ion backstreaming velocity of $V_{||} = 1.4V_{SW}$ for cone angle greater than 45°. The ion foreshock

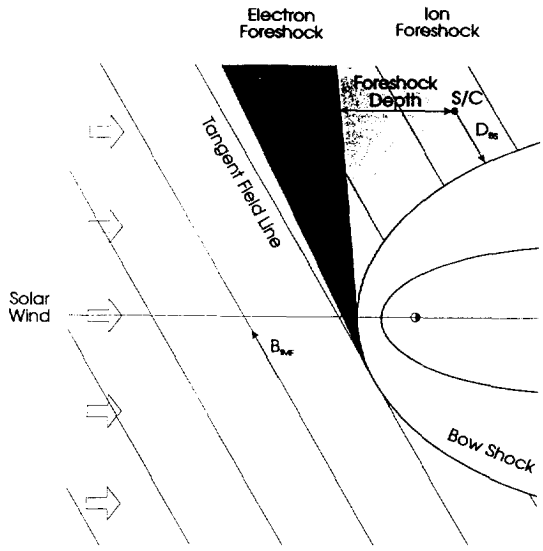

Figure 1: Schematic of foreshock geometry used in this study. The coordinate system is in the V-B plane.

depth is measured along the solar wind flow direction from ion foreshock boundary to spacecraft position. The missing of depth data implies that either the S/C was out of ion foreshock or the IMF cone angle less than 45° when we were not able to define the ion foreshock. Figure 1 shows our foreshock geometry. The θ_{BN} is the angle between the IMF and the bow shock normal. D_{BS} is measured along the IMF from bow shock to spacecraft position.

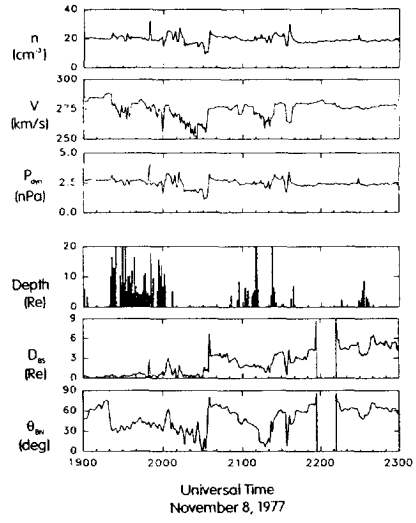

Figure 2: Upper three panels show the observed solar wind density, velocity and inferred dynamic pressure. The calculated ion foreshock depth, D_{BS} and θ_{bn} are shown in the lower three panels.

An example showing solar wind deceleration is shown in Figure 2. The upper three panels show the observed solar wind density, velocity and inferred dynamic pressure. The calculated foreshock depth, D_{BS} and θ_{BN} are shown in the lower three panels. The missing of depth data implies that either the S/C was out of ion foreshock or the IMF cone angle less than 45° (in these cases we were not able to define the ion foreshock). In order to find out the region where the solar wind decelerates, we plot this deceleration as a function of different foreshock geometry parameters, i.e., the depth, D_{BS}, and θ_{BN}. For this study, we have selected 4 orbits where the solar wind conditions were nearly constant. Thus the change of solar wind speed is primarily related to the geometry in the foreshock, e.g. the different depth from the foreshock boundary and different distance from the bow shock. The 4 orbits considered here are: November 8 (from 1900 UT to 2300 UT), November

18 (from 1400 UT to 1800 UT), December 1 (from 0600 UT to 1600 UT) and December 6 (from 0400 UT to 1400 UT).

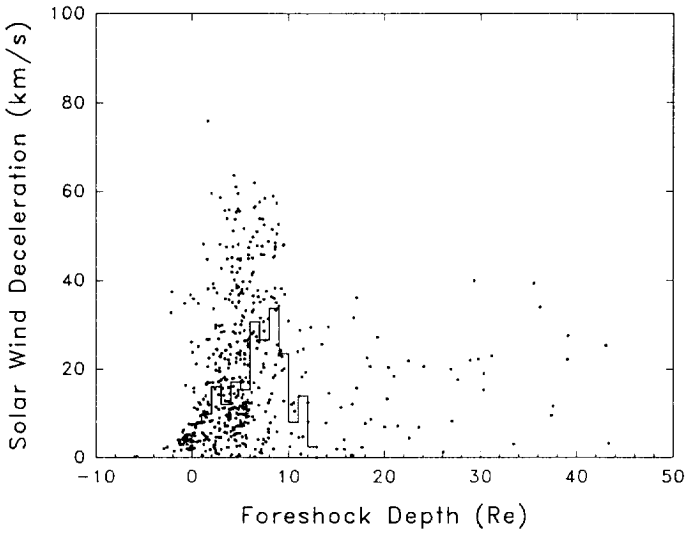

Figure 3: Scatter plot showing the dependence of the solar wind deceleration on the ion foreshock depth. The solid lines are the medians of the decelerations every 1 R_E in foreshock depth. While most of the decelerations occur within 10 R_E downstream of the ion foreshock, the median shows the maximum deceleration at 6-10 R_E.

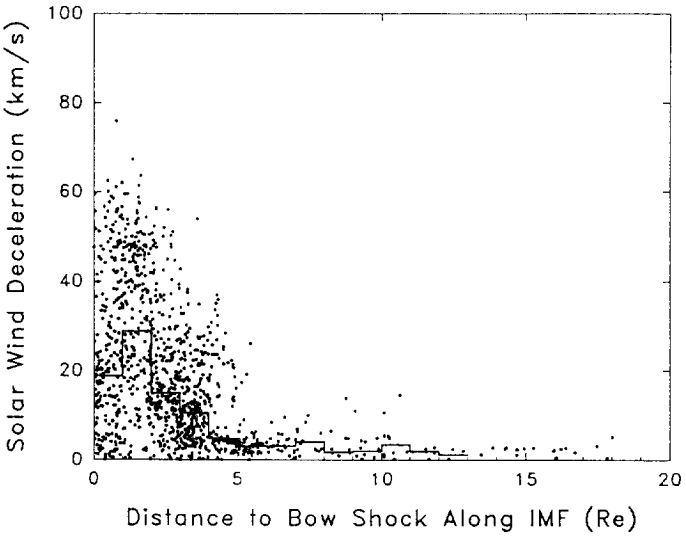

Figure 4: Solar wind deceleration as a function of the distance to bow shock along IMF. The solid lines are the medians of the decelerations every 1 R_E in D_{BS}. The deceleration is seen to be a maximum near the bow shock and decreases with the distance farther from the bow shock. The deceleration stops when D_{BS} reaches 5 R_E.

Figure 3 is a scatter plot showing the dependence of the solar wind deceleration on the ion foreshock depth. The solid lines are the medians from the scatter plot taken in 1 R_E bins. While most of the deceleration occurs within 10 R_E downstream of the ion foreshock, the median shows the maximum deceleration at 6-10 R_E. In Figure 4 we plot solar wind deceleration as a function of the distance to bow shock along IMF, D_{BS}. The deceleration is seen to be a maximum near the bow shock and decreases with the distance farther from the bow shock. The deceleration stops when Dbs reaches 5 R_E. In Figure 5 we show solar wind deceleration as a function of θ_{BN}. The solar wind deceleration starts around θ_{BN} of 50° where the ULF foreshock starts /8/. We see the solar wind decelerates most upstream the quasi-parallel shock.

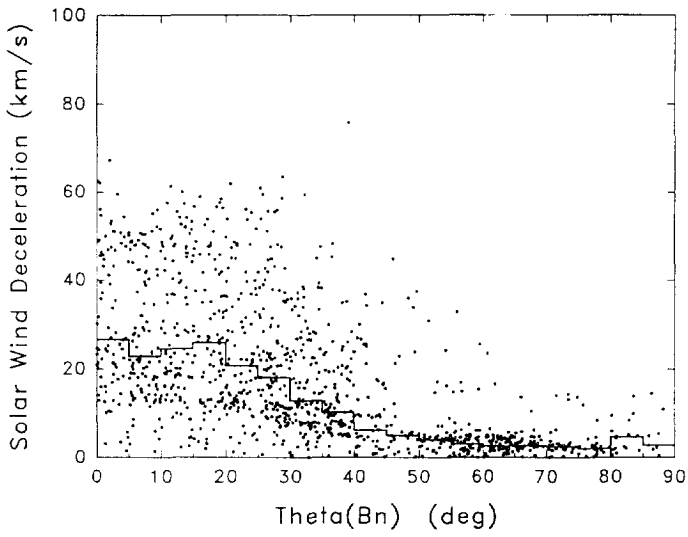

Figure 5: Solar wind deceleration as function of θ_{BN}. The solid lines are the medians of the decelerations every 5° of θ_{BN}. The solar wind deceleration starts around θ_{BN} of 50° where the ULF foreshock starts /8/.

CONCLUSIONS

We have examined the solar wind deceleration in the Earth's foreshock region and determined how the solar wind speed varies in the foreshock region. The deceleration occurs mainly within 10 R_E downstream of the foreshock when the cone angle greater than 45°. The solar wind speed decreases most in front of the quasi-parallel bow shock. Along the IMF direction, this deceleration is seen to be a maximum near the bow shock and stops when the distance from bow shock reaches 5 R_E. In front of the quasi-parallel bow shock, we observe large decreases of solar wind velocity as much as 60 km/s. Such solar wind velocity decelerations may result in pressure perturbations which could create significant effects on the magnetopause.

ACKNOWLEDGMENTS

The work at UCLA was supported by NASA grant NAGW-3477. Useful discussions are acknowledged with G. Le and G. K. Crawford.

REFERENCES

1. S. J. Bame, J. R. Asbridge, W. C. Feldman, J. T. Gosling, G. Paschmann and N. Sckopke, Deceleration of the solar wind upstream from the Earth's bow shock and the origin of diffuse upstream ions, *J. Geophys. Res., 85*, 2981, 1980.
2. C. Bonifazi, G. Moreno, A. J. Lazarus and J. D. Sullivan, Deceration of the solar wind in the Earth's foreshock region: Isee 2 and Imp 8 observations, *J. Geophys. Res., 85*, 6031, 1980.
3. C. Bonifazi, G. Moreno, C. T. Russell, A. J. Lazarus and J. D. Sullivan, Solar wind deceleration and MHD turbulence in the Earth's foreshock region: ISEE 1 and 2 and IMP 8 observations, *J. Geophys. Res., 88*, 2029, 1983.
4. V. Formisano and E. Amata, Solar wind interation with the Earth's magnetic Field 4. Preshock perturbation of the solar wind, *J. Geophys. Res., 81*, 3907, 1976.
5. D. H. Fairfield, W. Baumjohann, G. Paschmann, H. Lühr and D. G. Sibeck, Upstream pressure variations associated with the bow shock and their effects on the magnetosphere, *J. Geophys. Res., 95*, 3773, 1990.
6. D. H. Fairfield, Average and unusual locations of the Earth's magnetopause and bow shock, *J. Geophys. Res., 76*, 6700, 1971.
7. E. W. Greenstadt, and L. W. Baum, Earth's compressional foreshock boundary revisited: Observations by the ISEE 1 magnetometer, *J. Geophys. Res., 91*, 9001, 1986.
8. G. Le and C. T. Russell, A study of ULF wave foreshock morphology–1: ULF foreshock boundary, *Planet. Space Sci., 40*, 1203, 1992.